Renewable Energy 227 (2024) 120506

Contents lists available at ScienceDirect

Renewable Energy

journal homepage: www.elsevier.com/locate/renene

Control co-design for wave energy farms: Optimisation of array layout and mooring configuration in a realistic wave climate

Yerai Peña-Sanchez [a,b,*], Demián García-Violini [b,c,d], Markel Penalba [a,e], Ander Zarketa-Astigarraga [a], Francesco Ferri [f], Vincenzo Nava [g,h], John V. Ringwood [b]

[a] Fluid Mechanics Department, Mondragon University, Loramendi 4, 20500 Arrasate, Spain
[b] Centre for Ocean Energy Research, Maynooth University, Maynooth, Ireland
[c] Departamento de Ciencia y Tecnología, Universidad Nacional de Quilmes, Roque Saenz Peña 352, Bernal B1876, Argentina
[d] Consejo Nacional de Investigaciones Científicas y Técnicas (CONICET), Argentina
[e] Ikerbasque, Basque Foundation for Science, Euskadi Plaza 5, 48011 Bilbao, Spain
[f] Department of the Built Environment, Aalborg University, Aalborg, Denmark
[g] Basque Center for Applied Mathematics (BCAM), Mazarredo Zumarkalea 14, Bilbao, Spain
[h] TECNALIA, Basque Research and Technology Alliance (BRTA), Astondo Bidea, Edificio 700, Derio, 48160, Spain

ARTICLE INFO

Keywords:
Wave energy
Wave farms
Control co-design
Mooring lines
Optimisation
Techno-economics

ABSTRACT

This paper presents a novel Control Co-Design (CCD) methodology aimed at economically optimising the layout of wave energy converter (WEC) arrays. CCD ensures the synergy of optimised WEC and array parameters with the final control strategy, resulting in a comprehensive and efficient design of the array. By integrating a spectral-based control strategy into the array layout design, this study pursues the twin objectives of maximising energy absorption while reducing costs. To prove the performance of the proposed CCD methodology, an application case is proposed where the inter-device distance, alignment, and mooring configuration of a five-device array, considering realistic wave scenarios, are optimised. Energy capture and system cost evaluations are conducted, with results emphasising the significance of incorporating advanced control strategies in the design phase to improve energy absorption and reduce costs. With the application case, the study demonstrates that the optimal layout of a WEC array considering economic factors may differ from the optimal from purely technical factors, such as energy absorption, in the analysed case.

1. Introduction

In the pursuit of a sustainable, carbon-neutral global energy system, a significant expansion of renewable energy sources is paramount, marking a vital step away from fossil fuels. This transition aligns with the objectives outlined in both the Paris Agreement [1] and the latest assessment by the Intergovernmental Panel on Climate Change (IPCC) [2], aiming to mitigate the severe impacts of climate change [3]. Wind and solar energy technologies are already mature and reliable, but the massive upscaling to expedite this transition effectively will require the support of additional and diverse sources of energy. For example, the International Renewable Energy Agency (IRENA) estimates a staggering 14 TW increase in global renewable energy installed capacity requirement by 2050 [4]. This underlines the sheer magnitude of the challenge, for which the International Energy Agency predicts that roughly 45% of CO_2 emissions reduction by 2050 will be attributed to technologies still in the developmental stage [5]. In this context, offshore renewable energy (ORE) technologies, emerge as a promising alternative. Wave and tidal energy, though in early stages of development, are anticipated to make substantial contributions to the future energy mix [6,7], with the ambition to achieve over 300 GW of installed power, saving 500 Mt of carbon emission, by 2050.

The potential of ocean waves is enormous, but wave energy technology is still unprepared for its commercialisation, with all the currently existing projects (about 2.5 MW of total installed capacity worldwide) targeting research and demonstration [8]. At the current state of development, one can say that wave power is expected to have a different role in the energy mix, such as providing energy to isolated islands [9] or supplying a more reliable, less variable and more predictable energy source [10,11]. Additionally, compared to other renewable resources, wave energy has an advantage in predictability [12].

The future of wave energy predominantly hinges on wave energy converter (WEC) arrays, considering, among others, the limited power output of individual devices, the economies of scale in operation and

* Corresponding author.
E-mail address: ypena@mondragon.edu (Y. Peña-Sanchez).

https://doi.org/10.1016/j.renene.2024.120506
Received 15 October 2023; Received in revised form 23 January 2024; Accepted 15 April 2024
Available online 17 April 2024

maintenance (O&M) requirements [13]. In addition, IRENA has recently published a set of recommendations to enable the economic viability of wave energy, encouraging larger deployments that will enable significant cost reductions (to about 100 €/MWh) [14]. Nowadays, key research and development efforts are mostly directed towards optimising the size and arrangement of these WEC arrays [8].

Commonly, the optimisation of WEC arrays in the literature focuses on layout optimisation based on pure hydrodynamic optimisation [15,16], to maximise the constructive interaction among the devices or minimise the destructive interaction. Given the high computational cost of simulation with several WECs, different approaches from analytical to numerical to experimental methods [15] have been employed. In particular, the studies carried out using numerical models, are usually limited by the computational cost. One of the most common approaches, based on numerical models, is using boundary element method (BEM) solvers, such as NEMOH [17] or WAMIT [18], which consider the effects of diffracted and radiated wave fields within the array. However, these numerical models are computationally expensive, especially with relatively large arrays. Overall, other than for optimisation purposes, numerical models have been used to characterise the performance of WEC arrays, from the analysis of basic hydrodynamic interaction effects [19] to the assessment of different layouts in realistic wave climates [20–22].

However, the hydrodynamic performance of WEC and WEC arrays is often optimised either under uncontrolled [19] or passive control conditions [20–22], resulting in under-excited WECs for which the hydrodynamic interaction effects are relatively mild. Garcia-Rosa et al. [16] demonstrate that the behaviour of individual WECs under different control techniques can greatly influence the expected hydrodynamic interaction between devices, potentially shifting destructive interactions into constructive ones. This has a substantial impact on the overall performance of the array, underscoring the importance of carefully considering the control strategy in WEC array layout design. Such a mismatch between the behaviour of the (optimised) WEC design and the behaviour when considering advanced control is addressed by applying design constraints to the controller, which may lead to sub-optimal results [23].

To address such a challenge, control co-design (CCD) [24] of WECs or WEC arrays [25], where energy maximising control strategies are incorporated into the optimisation loop from the early stages, has recently gained popularity as a more integrative approach. In other words, this design paradigm emphasises a *control-informed* optimisation approach. Several studies in the literature have demonstrated the benefits of CCD for the optimisation of different WEC-related parameters. For example, [25] highlights that CCD strategies contribute significantly to achieving an optimal structural design for the absorber geometry, aligning it with the energy-maximising control scheme. Another interesting example is [26], where the authors optimise the power take-off (PTO) configuration considering a spectral-control technique.

Regardless of the selected modelling approach and control strategy, the hydrodynamic performance of WEC arrays, considering interaction effects among the devices in the array, is commonly quantified by means of the q-factor [27]. This factor compares the total energy absorbed by the entire array (E_{array}) to the energy absorption of the same number of isolated devices:

$$\mathrm{q} = \frac{E_{array}}{n_{\mathrm{b}} E_{\mathrm{isol}}}, \tag{1}$$

where E_{isol} is the energy absorbed by an isolated device and n_{b} the number of bodies composing the array. Hence, the q-factor can yield $\mathrm{q} > 1$, $\mathrm{q} = 1$, or $\mathrm{q} < 1$, inferring constructive, neutral and destructive hydrodynamic interactions, respectively.

Although specific separation between devices can theoretically lead to constructive hydrodynamic interaction, the q-factor alone is not expected to exclusively determine the optimal design of array layouts, since this will be mostly influenced by significant cost factors such as moorings and electrical interconnection. Yet, these two aspects are commonly neglected in the literature when the optimisation of a WEC array is considered. In that light, some authors are studying shared mooring lines in WEC arrays such as [28–30]. In particular, economic aspects are considered in [29,30], but no optimisation is performed. In contrast, the optimisation of mooring lines is considered in [31], but a single device is considered. However, none of the mentioned studies considers advanced control strategies for the WEC array.

To the best of the authors' knowledge, there are no studies in the literature that consider optimal-control-informed optimisation which couples array layouts and mooring systems, including shared mooring configurations, from an economic perspective, apart from a preliminary study by the same authors [32]. However, it should be noted that there are other studies optimising WEC array layout from an economic aspect, but most consider simple passive/reactive control strategies, such as [33–35], rather than optimal control strategies, which may alter the obtained results. The present paper significantly extends the CCD framework for WEC arrays presented in [32] by (i) increasing the size of the WEC array to include 5 devices as suggested in [22], (ii) studying different array configurations, (iii) considering a realistic wave climate with all the relevant sea states, and (iv) incorporating a realistic mooring configuration following the KARRATU concept suggested in [28].

The remainder of the paper is laid out as follows: Section 2 describes the WEC array numerical model employed in this study, along with the introduction of the tool considered to compute the hydrodynamic parameters of the WEC arrays; Sections 3 and 4 outline the spectral control method, defining the objective function and the CCD strategy, respectively. Once the general aspects of the proposed CCD approach are introduced, Section 5 introduces the considered case study, where the specific deployment site, WEC design, mooring configuration, and a way to compute the array cost are introduced in Sections 5.1, 5.2, 5.3, and 5.4, respectively. However, it should be noted that the methodology proposed in Sections 2–4 is general and could be applied to a different case study if properly defined. Finally, Section 6 illustrates the most relevant results, and Section 7 draws the main conclusions of the study.

2. WEC array hydrodynamic model

In this section, the considered dynamic model of the WEC array, which accounts for the interactions between the fluid (water) and the floating bodies, is introduced. This model also considers interactions between various bodies due to the radiated and diffracted waves originating from the other devices in the array. Note that, to simplify the study, but without loss of generality, a single DoF (heave) is considered for the motion of the devices composing the array. Thus, the model is formulated, in the time-domain, based on Newton's second law, as follows:

$$\left(m + \mu_{\infty}\right) \ddot{x}(t) = f_{\mathrm{e}}(t) - f_{\mathrm{h}}(t) - f_{\mathrm{r}}(t) - f_{\mathrm{m}}(t) - f_{\mathrm{u}}(t), \tag{2}$$

where the mass matrix $m \in \mathbb{R}^{n_{\mathrm{b}} \times n_{\mathrm{b}}}$ holds the mass of each device on its diagonal, with zeros elsewhere. The infinite frequency added mass of the WECs, denoted as $\mu_{\infty} \in \mathbb{R}^{n_{\mathrm{b}} \times n_{\mathrm{b}}}$, encompasses both the diagonal elements representing the infinite frequency added mass of the individual WECs and the off-diagonal elements accounting for the interactions. The state vectors, $x(t) \in \mathbb{R}^{n_{\mathrm{b}}}$, $\dot{x}(t) \in \mathbb{R}^{n_{\mathrm{b}}}$ (or equivalently, $v(t)$), and $\ddot{x}(t) \in \mathbb{R}^{n_{\mathrm{b}}}$ (or equivalently, $a(t)$), contain information about the position, velocity, and acceleration of the WECs, respectively. The forces acting on the WECs, as introduced in Eq. (2), are defined as:

- the hydrostatic force $f_{\mathrm{h}}(t)$ is represented as $f_{\mathrm{h}}(t) = s_{\mathrm{h}} x(t)$, with $s_{\mathrm{h}} \in \mathbb{R}^{n_{\mathrm{b}} \times n_{\mathrm{b}}}$ the hydrostatic stiffness matrix;
- the radiation force is calculated using a convolution integral as $f_{\mathrm{r}}(t) = k_{\mathrm{r}}(t) * \dot{x}(t)$, with $k_{\mathrm{r}}(t)$ the radiation convolution kernel;

- the mooring force, modelled as a spring–damper system, is expressed as $f_{\mathrm{m}}(t) = s_{\mathrm{m}}x(t) + b_{\mathrm{m}}\dot{x}(t)$, where $s_{\mathrm{m}} \in \mathbb{R}^{n_{\mathrm{b}}\times n_{\mathrm{b}}}$ and $b_{\mathrm{m}} \in \mathbb{R}^{n_{\mathrm{b}}\times n_{\mathrm{b}}}$ represent the mooring stiffness and damping matrices;
- and the wave excitation and PTO control force are defined as $f_{\mathrm{e}}(t) \in \mathbb{R}^{n_{\mathrm{b}}}$ and $f_{\mathrm{u}}(t) \in \mathbb{R}^{n_{\mathrm{b}}}$, respectively.

Note that both the infinite frequency added mass matrix (μ_∞) and the radiation convolution kernel matrix (k_{r}) can be calculated based on the frequency-domain radiation added-mass and damping hydrodynamic coefficients ($A_{\mathrm{r}}(\omega) \in \mathbb{R}^{n_{\mathrm{b}}\times n_{\mathrm{b}}}$ and $B_{\mathrm{r}}(\omega) \in \mathbb{R}^{n_{\mathrm{b}}\times n_{\mathrm{b}}}$) using Ogilvie's relations [36], and Eq. (2) can be defined in the frequency-domain using the force-to-velocity description of the array [37] as:

$$V(\omega) = Z_i^{-1}(\omega)\left[F_{\mathrm{e}}(\omega) - F_{\mathrm{u}}(\omega)\right], \tag{3}$$

where $Z_i(\omega) \in \mathbb{I}^{n_{\mathrm{b}}\times n_{\mathrm{b}}}$ is the intrinsic impedance of the system, which can be defined as follows:

$$Z_i(\omega) = B_{\mathrm{r}}(\omega) + b_{\mathrm{m}} + \jmath\omega\left(m + A_{\mathrm{r}}(\omega) - \frac{s_{\mathrm{h}} + s_{\mathrm{m}}}{\omega^2}\right). \tag{4}$$

The force-to-velocity transfer function [38], essential for control design purposes, can now be defined based on Eq. (4) as

$$G_{\mathrm{fv}}(\omega) = \jmath\omega[-\omega^2(m + \mu_\infty) + \jmath\omega(H_{\mathrm{r}}(\omega) + b_{\mathrm{m}}) + s_{\mathrm{h}} + s_{\mathrm{m}}]^{-1}, \tag{5}$$

where all the required frequency-domain hydrodynamic parameters can be determined using BEM solvers.

Boundary element methods have the advantage of being able to cope with a 3D formulation of the hydrodynamic problem, which allows the calculation of any WEC geometry. However, they become too computationally expensive when dealing with many interacting WECs. On the other hand, Kagemoto and Yue [39] came up with a direct matrix method approach, comparable to BEM codes in terms of capabilities and accuracy of the results, which significantly reduces the computation time. Such an approach was later combined with results from conventional BEM software, allowing the solution for WECs of any shape and mode of operation [40]. In particular, to reduce the computational effort for large arrays, the direct matrix method estimates the wave field for each WEC as a summation of the undisturbed incident wave field plus the wave scattered and radiated by other devices in the array.

These array effects are modelled using partial waves whose amplitude is obtained by fitting the velocity potential of the device obtained by BEM software. In general, for simple WEC geometries, only a few partial waves are sufficient to reproduce the wave field accurately while, for complex geometries, 10 or 20 partial waves are needed. To this extent, the hydrodynamic effect of a single body is fully represented by few partial waves, compared to a standard BEM where the hydrodynamic effects are estimated from the amplitude of the source potential, which has to be solved for each mesh node (with hundreds to thousands of elements). Hence, a version of the BEM solver NEMOH [17], including the direct matrix method for WEC arrays, is considered here to compute the hydrodynamic parameters of all the analysed cases.

3. Spectral control

This section offers an overview of the spectral control strategy implemented in this study. Spectral controllers excel in managing physical constraints and can theoretically achieve optimal solutions (based on the chosen resolution of the basis functions) [41], with reduced computation complexity compared to, say, model predictive control (MPC) strategies [42]. For a deeper understanding, Sections 3.1 and 3.2 delve into the general control objectives for WECs and the fundamental principles of spectral controllers, respectively.

3.1. WEC control objective function

For the case of a WEC array system, subject to an external excitation force $f_{\mathrm{e}}(t)$ and controlled by a PTO force $f_{\mathrm{u}}(t)$, the total absorbed energy for all devices in the array ($E \in \mathbb{R}$) over the time interval $[0, T]$ can be computed as follows:

$$E = -\int_0^T P(t)dt = -\int_0^T \dot{x}^{\intercal}(t) f_{\mathrm{u}}(t)dt, \tag{6}$$

where $P(t) \in \mathbb{R}$ is the (instantaneous) absorbed power. Thus, the control problem is commonly expressed as

$$\max_{f_{\mathrm{u}}(t)} \quad -\int_0^T \dot{x}(t)^{\intercal} f_{\mathrm{u}}(t)dt \qquad \text{subject to} \quad \begin{cases} \dot{\mathrm{x}} = \mathcal{F}(\mathrm{x}, f_{\mathrm{u}}, f_{\mathrm{e}}) \\ \dot{x} = \mathcal{G}(\mathrm{x}) \\ C \end{cases} \tag{7}$$

with $\mathcal{F}(x, f_{\mathrm{u}}, f_{\mathrm{e}})$ representing the multiple-input multiple-output (MIMO) state-space system of the WEC, derived from Eq. (2), $\mathcal{G}(\mathrm{x})$ the output mapping of the state space, where $\mathrm{x} \mapsto \dot{x}$, and the set of considered constraints, denoted as C, is limited to displacement and PTO force constraints, specifically $x_{\min} \le x(t) \le x_{\max}$ and $f_{\min} \le f_{\mathrm{u}}(t) \le f_{\max}$, respectively.

3.2. Spectral control

The initial step entails discretising the optimal control formulation derived from Eq. (7) within the spectral domain. This discretisation procedure involves projecting the state vector $x(t)$ and the control force f_{u} onto an orthonormal vector space with a dimension of N, which is achieved through a linear combination of orthogonal basis functions, denoted as $\boldsymbol{\Phi} = [\phi_1, \phi_2, \ldots, \phi_N]$. Among the potential basis functions, the Fourier basis is a pertinent selection, inspired by the harmonic characteristics of the WEC variables. Consequently, the approximation of the states and control force takes the form of:

$$\begin{aligned} x(t) &\approx \mathrm{x}^N(t) = \hat{\mathrm{x}}\boldsymbol{\Phi}(t)^{\intercal}, \\ f_{\mathrm{u}}(t) &\approx \mathrm{f}_{\mathrm{u}}^N(t) = \hat{\mathrm{f}}_{\mathrm{u}}\boldsymbol{\Phi}(t)^{\intercal}, \end{aligned} \tag{8}$$

with both coefficient vectors $\hat{\mathrm{x}} = [\hat{x}_1, \hat{x}_2, \ldots, \hat{x}_N]$ and $\hat{\mathrm{f}}_{\mathrm{u}} = [\hat{f}_{\mathrm{u}1}, \hat{f}_{\mathrm{u}2}, \ldots, \hat{f}_{\mathrm{u}N}]$ as elements of the real vector space $\mathbb{R}^{n_{\mathrm{b}}\times N}$. Considering such a (pseudo-) spectral framework, the WEC array equation of motion can be approximated [43] as follows:

$$\hat{\mathrm{v}} = (\hat{\mathrm{f}}_{\mathrm{e}} - \hat{\mathrm{f}}_{\mathrm{u}})\mathrm{G}_{\mathrm{o}}. \tag{9}$$

In Eq. (9), the coefficient vector $\hat{\mathrm{v}} = [v_1, v_2, \ldots, v_N]^{\intercal}$ serves as an approximation for the velocities of the WECs in the array $\mathrm{v}(t)$, while G_{o} denotes the force-to-velocity system model. Furthermore, $\hat{\mathrm{f}}\mathrm{e} = [\hat{f}_{\mathrm{e}1}, \hat{f}_{\mathrm{e}2}, \ldots, \hat{f}_{\mathrm{e}N}]^{\intercal}$ represents the coefficient set $\hat{f}_{\mathrm{e}1}, \hat{f}_{\mathrm{e}2}, \ldots, \hat{f}_{\mathrm{e}N}$ utilised to approximate the excitation forces affecting the different WECs.

Then, considering the mathematical properties of the basis functions $\boldsymbol{\Phi}_j$ [44], one can approximate the objective function in Eq. (6) as

$$E \approx J_N = \int_0^T \hat{\mathrm{f}}_{\mathrm{u}}\boldsymbol{\Phi}(t)^{\intercal}\boldsymbol{\Phi}(t)\hat{\mathrm{v}}^{\intercal} = -\frac{T}{2}\hat{\mathrm{f}}_{\mathrm{u}}\hat{\mathrm{v}}^{\intercal}, \tag{10}$$

which converts, via an algebraic mapping, the integral relationship expressed in Eq. (6). Thus, with Eqs. (9) and (10), the controller objective function can be expressed now in terms of the coefficient vectors $\hat{\mathrm{f}}_{\mathrm{u}}$, $\hat{\mathrm{f}}_{\mathrm{e}}$, and the force-to-velocity system model G_{o} as

$$J_N = -(\hat{\mathrm{f}}_{\mathrm{e}} - \hat{\mathrm{f}}_{\mathrm{u}})\mathrm{G}_{\mathrm{o}}\frac{T}{2}\hat{\mathrm{f}}_{\mathrm{u}}^{\intercal}. \tag{11}$$

Finally, the control optimisation problem for WEC arrays can now be expressed as

$$\begin{aligned} \hat{\mathrm{f}}_{\mathrm{u}}^{\star} \leftarrow \max_{\hat{\mathrm{f}}_{\mathrm{u}}\in\mathbb{R}^N} \quad & J_N \\ \text{subject to:} \quad & C. \end{aligned} \tag{12}$$

In essence, the optimisation problem described in Eq. (12) constitutes a quadratic optimisation problem involving the PTO force $\hat{\mathrm{f}}_{\mathrm{u}}$. Such a problem is subject to a set of constraints C, which stem from the physical limitations inherent to the WEC system. In the specific application discussed in Section 5, the set of constraints C can be formulated based on parameters such as the maximum device displacement ($X_{\max}$), maximum PTO force ($F_{\max}$), and maximum velocity ($V_{\max}$).

To address the constrained optimisation problem defined in Eq. (12), a collocation technique is employed. In this approach, the constraints are enforced at specific time points referred to as collocation points. When considering common constraints like $X_{\max}$ and $F_{\max}$, the set of constraints C in Eq. (7) can be reformulated as a set of linear inequality constraints [45] as shown below:

$$C := \begin{bmatrix} A_{\mathrm{u}} \\ A_{\mathrm{x}} \end{bmatrix} \hat{\mathrm{f}}_{\mathrm{u}}^{\intercal} \leq \begin{bmatrix} b_{\mathrm{u}} \\ b_{\mathrm{x}} \end{bmatrix}, \tag{13}$$

where

$$\begin{aligned} A_{\mathrm{u}} &= \begin{bmatrix} \boldsymbol{\Phi}(\mathbf{T}_c) \\ -\boldsymbol{\Phi}(\mathbf{T}_c) \end{bmatrix}, \quad A_{\mathrm{x}} = \begin{bmatrix} \boldsymbol{\Phi}(\mathbf{T}_c)\mathrm{G}_{\mathrm{o}} \\ -\boldsymbol{\Phi}(\mathbf{T}_c)\mathrm{G}_{\mathrm{o}} \end{bmatrix}, \\ b_{\mathrm{u}} &= \begin{bmatrix} F_{\max}\hat{\mathbf{1}} \\ F_{\max}\hat{\mathbf{1}} \end{bmatrix}, \quad b_{\mathrm{x}} = \begin{bmatrix} X_{\max}\hat{\mathbf{1}} - \boldsymbol{\Phi}(\mathbf{T}_c)\hat{\mathrm{f}}_{\mathrm{e}} \\ X_{\max}\hat{\mathbf{1}} + \boldsymbol{\Phi}(\mathbf{T}_c)\hat{\mathrm{f}}_{\mathrm{e}} \end{bmatrix}, \end{aligned} \tag{14}$$

where $\hat{\mathbf{1}} \in \mathbb{R}^{2n_{\mathrm{c}}n_{\mathrm{b}}\times 1}$ is a block diagonal matrix of ones with n_{c} the number of chosen collocation points and $\mathbf{T}_c = \left[t_1, t_2, \ldots t_{n_{\mathrm{c}}}\right]$ a vector containing the specific time instants at which the constraints are enforced. Leveraging the defined collocation points, general-purpose optimisation solvers, particularly those tailored for quadratic programming (QP), can be applied to address the presented problem.

4. Control co-design algorithm

In this section, the formulation and solution approach for the WEC array CCD problem are introduced. Generally, it is possible to formulate the WEC array CCD scheme as

$$\begin{aligned} \rho^{\mathrm{opt}} \leftarrow \quad & \underset{\rho\in\mathbb{R}^N}{\text{Optimise}} && \Psi \\ & \text{subject to:} \quad \underset{\substack{\hat{\mathrm{f}}_{\mathrm{u}}\in\mathbb{R}^N \\ C}}{\max} && J_N(\rho). \end{aligned} \tag{15}$$

In this case, the optimisation problem aims to minimise or maximise (depending on the definition) the objective function Ψ with respect to the variable ρ, while adhering to the constraints defined by the spectral controller detailed in Eq. (12). It should be noted that the structure of the objective function Ψ is contingent upon the unique specifications and needs of the application. In this analysis, the objective function Ψ will encompass the economic evaluation of each array layout ρ, taking into account the optimised control actions for each device in the array.

4.1. CCD objective function definition

As highlighted in the introduction, one of the paramount challenges within wave energy is the substantial reduction of overall expense associated with WEC arrays to achieve economic viability. In the existing literature, the levelised cost of energy (LCoE) stands as the main metric employed to assess the economic viability of diverse energy sources. Thus, the present study introduces an innovative optimisation methodology aiming to determine the optimal configuration for WEC arrays, leveraging a metric derived from LCoE. Traditionally, LCoE (expressed in €/MWh) is articulated as follows:

$$\mathrm{LCoE} = \frac{\mathrm{CapEx} + \mathrm{OpEx}}{\text{Energy production}}, \tag{16}$$

where CapEx and OpEx refer to the capital and operational expenditure of the array, respectively, and the energy production is computed over the projected operational lifespan of the WEC array.

As mentioned in Section 1, this study exclusively concentrates on optimisation of the inter-device distance and orientation of a given WEC array layout, with a homogeneous set of WECs. Hence, the cost variations from one array layout to another will primarily affect CapEx. Thus, for this analysis, OpEx is presumed to be a fraction of CapEx, which ensures that OpEx does not exert any influence on the outcome of the optimal array layout. However, it is important to acknowledge that adjustments in the array layout may potentially influence device interaction, impacting WEC behaviour and, subsequently, operation and maintenance needs. Nevertheless, it is reasonable to assume that the costs associated with these effects are relatively negligible compared to CapEx.

The capital expenditure associated with WEC arrays can be further dissected into several components, including the expenses related to site leasing (LeEx), the expenses incurred during device commissioning (ComEx), and the cost of the devices (DevEx) themselves, which can also be subdivided into their individual components. Among such components, the mooring system of the array may exhibit variability depending on the layout under consideration, potentially influencing the cost calculations since, in certain layouts, WECs may share specific parts of the mooring system, such as the chain or the anchor. Since the present study maintains uniform devices across all layouts, most of the components of the WECs are common for all the scenarios and, hence, do not affect the obtained optimal layout. Therefore, for the sake of simplicity, such components of the WECs are excluded from this study. Consequently, the cost of devices in the array can, in this study, be defined as the cost of the mooring system. Note that, when sharing components of the mooring system, such as anchors, the cost savings extend beyond just the anchor itself. This includes the cost associated with its installation, which can be categorised as part of the commissioning cost (ComEx).

Finally, the sole commissioning expense taken into account pertains to the installation of the mooring anchor, since it is the only cost that fluctuates depending on the layout. Other commissioning expenses are presumed to remain constant irrespective of the layout under consideration and, hence, will not affect the obtained outcome of the analysis. Thus, it is possible to define a new performance function, similar to that in Eq. (16), as

$$\mathrm{LCoE}^* = \frac{\mathrm{CapEx}^*}{E}, \tag{17}$$

with the generated energy E as in Eq. (6), and CapEx* containing all the costs derived from the mooring system of the array (mooring lines and anchors), as well as the site leasing cost (which depends on the layout size).

4.2. CCD problem solution

The problem described in Eq. (15) is typically addressed, as documented in [24], through control-inspired, co-optimisation, or co-simulation approaches. In particular, co-simulation emerges as a potent methodology for discovering optimal solutions within the realm of CCD problems [24]. It facilitates a thorough analysis of system dynamics, streamlines the exploration of design alternatives, and shortens the design cycle. Co-simulation can seamlessly integrate models spanning multiple scales and physics domains, encompass optimisation algorithms and data-driven methodologies, and offer a modular approach to design. The interested reader is referred to [24] for more in-depth insights into CCD solution strategies.

In this study, a co-simulation approach is adopted to address the CCD problem outlined in Eq. (15). Ideally, this co-simulation method could be coupled with an optimal point search algorithm, such as linear or binary search techniques. However, for the sake of giving informative results for all potential array layouts, an exhaustive search procedure is considered here. This parametric study entails computing outcomes for every conceivable WEC array layout, ultimately revealing which configuration minimises the objective function described in

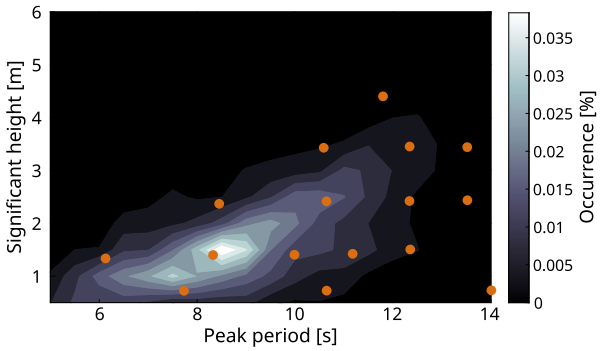

Fig. 1. Scatter diagram of the wave conditions at BIMEP with the chosen sea states denoted with orange dots [48].

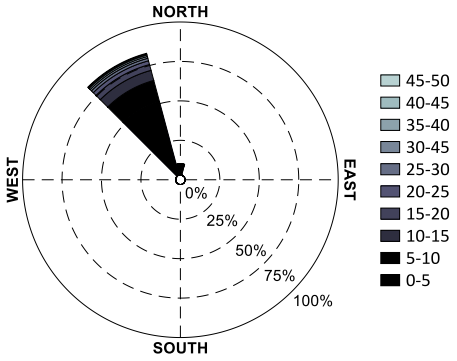

Fig. 2. Wind rose at BIMEP.

Section 4.1, but also showing sensitivity to parameter variation. The advantage of this approach lies in its ability to furnish a comprehensive overview of the search space.

5. Case study

In this section, an illustrative example is presented to emphasise the advantages of the CCD method introduced in this paper. This methodology is applied to a specific case study to demonstrate the benefits and potential enhancements that can be achieved by integrating advanced control strategies with system design, rather than relying on simple passive controllers. Through this example, the significance of incorporating control considerations from the early stages of system development is highlighted, leading to improved performance and optimised outcomes in practical applications.

5.1. Realistic climate

In this analysis, a comprehensive evaluation of the energy generated by the WEC array at a specific location is pursued. Thus, as mentioned in Section 4.1, the consideration of various sea states to assess the performance of a WEC array on a specific site is necessary, with these sea states being selected based on the probability distribution of their occurrence at the designated site, a representation commonly depicted using a scatter diagram [46]. It is important to note that while calculating energy production, a 20-year operational lifespan is assumed for the array but, for simplicity, no potential variations in sea state intensity over time are accounted for here (such as the potential increase in intensity and aggressiveness of sea states as time progresses, as illustrated in [47]).

For this study, the chosen location is BIMEP, an offshore test site located in the Bay of Biscay off the Basque coast [48]. In order to include the information of the site within the considered CCD problem, it is necessary to characterise the wave conditions of the given site with a finite number of sea states. To this end, the 16 most relevant sea states (from an electricity generation perspective [48]) have been chosen in this analysis, as shown in Fig. 1, to cover the wave conditions of the selected location in a computationally simplified manner.

In addition to accounting for the most significant sea states, it is imperative to take into consideration the various potential wave directions at a site to ensure the optimal layout of the array. In this particular scenario, as depicted in Fig. 2, it is evident that waves primarily approach BIMEP from a single direction. Therefore, for the CCD problem at hand, a single wave direction is considered. However, it should be noted that considering multiple wave headings would not alter the proposed CCD scheme, it would only affect the definition of the excitation force f_e introduced in Section 2.

Finally, in order to be statistically consistent, the results for each of the chosen sea states are derived by averaging the outcomes across several realisations of each sea state. For the current case study, it is found that 10 realisations with randomised seeds are enough to obtain statistically consistent values of the absorbed power for each sea state. Then, it is assumed that the acquired results are applicable for a specific number of days within the 20-year operational lifespan, depending on the frequency of occurrence of each sea state, as shown in Fig. 1.

5.2. WEC device and array

The WEC array considered here comprises five identical heaving point absorbers aligned in a linear array configuration. It should be noted that assuming the WECs exclusively exhibit heave motion represents a significant simplification since the optimisation algorithm incorporates the mooring system into the objective function, and takes into account that additional DoFs would considerably affect the mooring configuration selection. Furthermore, accounting for surge and sway motion would require careful consideration of the minimum inter-device distance to prevent collisions. However, for the purpose of this study, which aims to demonstrate the proposed methodology in a straightforward manner, the simplifying assumption that the WECs move solely in heave is retained.

The device selected for this analysis is inspired by the MARMOK-A-5 WEC, a spar-like floating oscillating water column (OWC) [49,50] developed by IDOM which was deployed at the BIMEP test site for over two and a half years using a mooring configuration similar to the one suggested here (see Section 5.3). However, due to the complexity associated with modelling an OWC concept, the device is simplified as a single-body cylindrical point absorber with the same geometric characteristics as the MARMOK-A-5 floater, shown in Fig. 3. Due to the geometric similarities, the hydrodynamic behaviour of the simplified device is expected to be similar to the MARMOK-A-5 WEC and, thus, conclusions extracted from the present study can be considered valid. Nevertheless, for correct optimisation of the layout for an array composed of MARMOK-A-5 devices, the correct hydrodynamic definition (a floating OWC) should be used.[1]

Furthermore, an increasing interest in arrays of similar devices can be found within the wave energy literature, *e.g.* [29] analysing different mooring configurations for similar devices in arrays of 5 devices and [22] using the same geometry approximation for assessing the performance of arrays of different sizes. In the current study, the array layout consists of 5 devices in line, as illustrated in Fig. 4. The decision is based on different studies in the literature as, for

[1] Or, conversely, an analysis should be carried out to see if the behaviour of the MARMOK-A-5 could be characterised using the considered simplified heaving point absorber along with a correction factor. However, assuming a consistent correction factor between devices, this will not affect the optimal answer achieved.

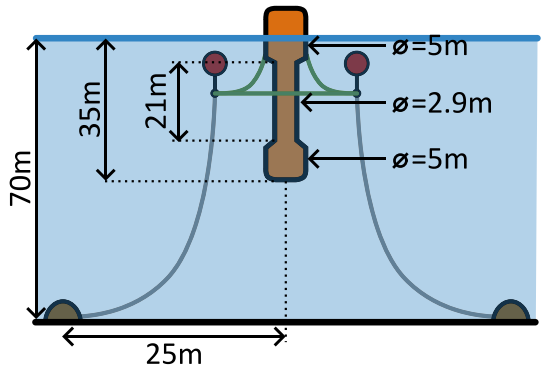

Fig. 3. Main dimensions of the considered WEC and mooring system (as introduced in Section 5.3).

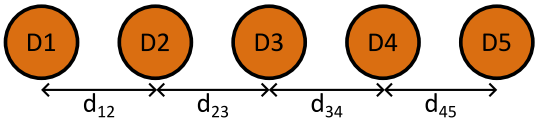

Fig. 4. WEC array layout considered in this study.

example, [28] where a similar array layout that uses the KARRATU mooring configuration is suggested. Furthermore, [22] concludes that small arrays of up to 5 devices are hydrodynamically more effective. In fact, [29] also suggests an array of 5 devices.

As mentioned before, the primary objective of this study is to demonstrate the applicability of the proposed CCD scheme for optimising array layouts. To achieve this, various inter-device distances and array alignments are considered for the layout depicted in Fig. 4. However, it should be noted that, in order to simplify the representation of the results (and reduce the number of cases), it is assumed that the array under study is symmetric for all the cases analysed, i.e. $d_{12} = d_{45}$ and $d_{23} = d_{34}$. Thus, a set of 19 different inter-device distances (ranging from 2 to 20ø) are considered here for d_{12} and d_{23}. Additionally, three different alignments of the array with respect to the incoming waves which, as mentioned in Section 5.1, are considered to have a single wave direction, are analysed. In particular, the three considered alignments are 0° (array perpendicular to wave direction, the wave front arrives at all the WECs at the same time), 45° (intermediate case), and 90° (in line with the wave direction, incoming waves travel from D1 to D5, see Fig. 4). Thus, the aforementioned inter-device distances and array alignments are assessed to determine the optimal array configuration for the BIMEP location. Finally, it should be noted that, as introduced in Section 3, a constraint on the maximum displacement is considered here, defined as $X_{\max} = 5$ m.

5.3. Mooring configurations: KARRATU

Several mooring configurations have been presented in the literature, paving the way towards the development of innovative solutions for the station keeping of ORE devices. The purpose of these innovations is to either reduce the cost of the mooring systems or enhance their performance, including offset reduction and peak load mitigation. Such innovative configurations range from simple chain catenaries anchored to the seabed to mixed material mooring lines connected by floating elements, clump weights, and novel elastomeric tethers [51].

Among the different solutions, KARRATU has been presented in the literature as a compliant modular mooring configuration. As shown in Fig. 5, it is composed of a square design of wires, whose corners are connected to fairleads of the device via polyester lines. At each corner, a floating surface buoy is located and connected to the seabed through a catenary chain. In [28], the KARRATU concept is introduced for an

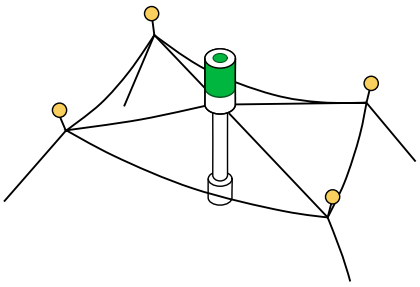

Fig. 5. Sketch of the KARRATU mooring configuration.
Source: Adapted from [53].

array of floating point absorbers. The main advantage of the KARRATU is the reduction of impedance and damping related to the mooring system while increasing the freedom of device movement. This concept has been successfully installed and tested for a single MARMOK-A-5 device during the EU-funded OPERA project [52].

5.4. LCoE* calculation

As introduced in Section 3.1, the only costs considered for the CCD problem are those that vary with the array layout: i.e. mooring and leasing costs. Thus, the costs associated with the KARRATU mooring system can be divided into the individual costs of different components: Anchors, catenary legs, surface buoys, umbilical cable, cables connecting the four surface buoys,[2] and the cables connecting the buoys with the WEC. It should be noted that the cost of the intra-array cables is not considered here, since it would depend on the selected connection configuration (in series or in parallel) and the location of the substation. Similarly, the cost of the dynamic cables connecting the devices to the static ones has not been included as it does not depend on the layout. Additionally, the cost of the surface buoys is also not considered, since it is negligible compared to the cost of the other components [54].

The array mooring configuration (and, hence, its cost) depends on the inter-device distances associated with each specific layout. Thus, as shown in Fig. 6, for any WEC pair, three different configurations are considered:

- If the inter-device distance between bodies i and j (d_{ij}) is larger than d_{an} (i.e. the distance between two subsequent anchors of the same WEC), the devices are moored in a separate fashion and, hence, each WEC has two independent mooring systems (see Fig. 6.a). In this case, the cost of the mooring for the two devices is given by:

$$\text{MooEx}^* = 2\left(4c_{an} + 4c_{ch}L_{ch} + 4c_{ss}L_{ss}\right), \tag{18}$$

  where c_{an} is the cost of each anchor, c_{ch} the cost per unit length of the chain used for the mooring legs, L_{ch} the length of such chains, c_{ss} the cost per unit length of the elastic fibre used for the square sides, and $L_{ss} = 2ø$ the length of each side.
- If $2ø < d_{ij} \leq d_{an}$, as shown in Fig. 6.b, the two WECs share two of the anchors but, apart from that, have their own separate mooring system. For this case, the cost of the mooring is defined as

$$\text{MooEx}^* = 6c_{an} + 8c_{ch}L_{ch} + 8c_{ss}L_{ss}. \tag{19}$$

- Finally, if the inter-device distance is 2ø, the KARRATU systems of the two devices are connected, sharing one of the square connectors side, two of the anchors and two of the mooring

[2] Note that the cost of such cables is not considered here, since it does not vary with the layout configuration.

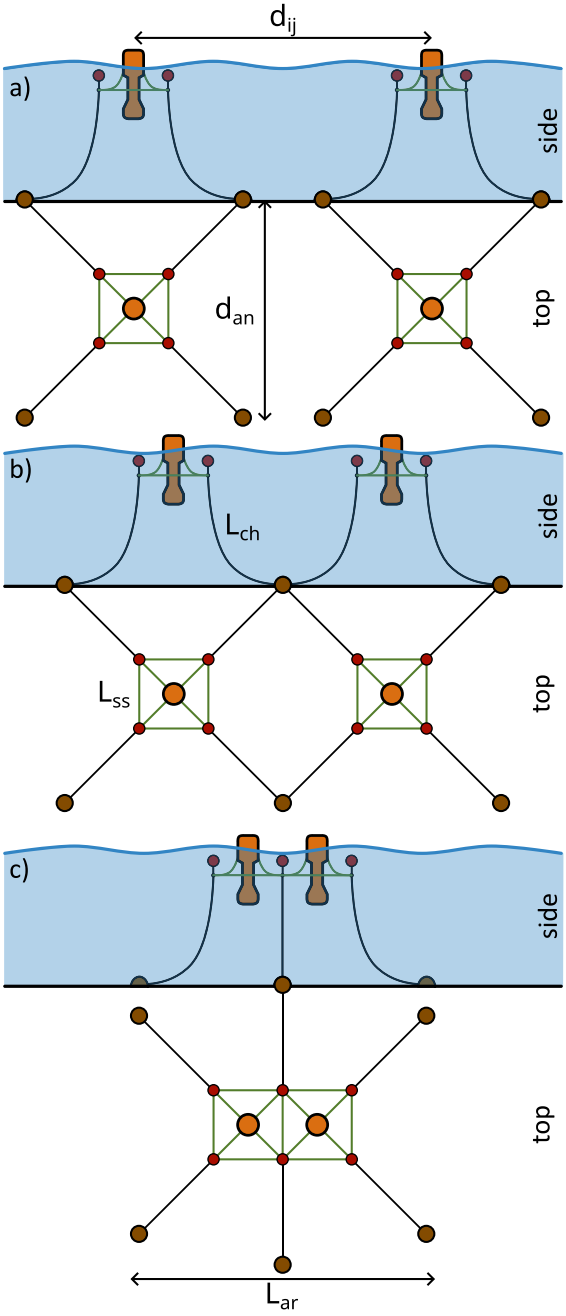

Fig. 6. Sketch of the different mooring configurations depending on the inter-device distance.

legs (as illustrated in Fig. 6.c). The mooring cost for this case is expressed as

$$\mathrm{MooEx}^* = 6c_{an} + 6c_{ch}L_{ch} + 7c_{ss}L_{ss}. \tag{20}$$

Note that, for the sake of simplicity, in this study, the previous configurations and mooring costs (as given in Eqs. (18)–(20)) are presented for a single pair of devices. However, in this analysis, five WECs are considered. Consequently, the total cost of the mooring systems of all five devices, for each given layout, is computed by combining the introduced three mooring configurations. Note that the choice of the mooring configurations for each layout depends on the specific inter-device distances of the layout being analysed.

The costs of the anchors (c_{an}), chain (c_{ch}), and elastic fiber (c_{ss}) are obtained from [54], and are presented in Table 1. It should be noted that, owing to the scarcity of accessible information on mooring costs for WECs, the costs outlined in [54] are incorporated here, despite that the primary focus of [54] is on floating offshore wind platforms. Regarding installation costs, those introduced in [54] are considered here, i.e c_{in} = 44 k€/anchor. Also, in this case, the cost of the anchors is kept constant regardless of the number of connected devices (1 or 2). Even though there could exist a specific case in which the force in the anchor increases because of having two devices connected to it, [55] shows that, for floating offshore platforms, among the several design load cases analysed, there is no case where the force in the anchor increases. Thus, it is a reasonable simplification to consider the same anchor for all cases.

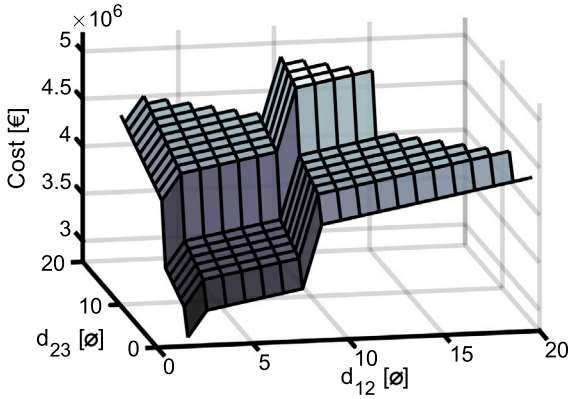

Fig. 7. Predicted costs for the various inter-device distances considered.

Table 1
Cost of the mooring components from [54].

Material	Cost
Anchor	114k €/anchor
Chain	755 €/m
Elastic fibre	182 €/m

Finally, the leasing cost of the deployment site is determined based on the approach described in [56], with the assumption that it constitutes roughly one-third of the total mooring system cost. Consequently, when considering an independent device with its own mooring system, the leasing cost per linear meter can be computed as follows:

$$c_{le} = \frac{4c_{an} + 4c_{ch}L_{ch} + 4c_{ss}L_{ss} + 4c_{in}}{3d_{an}}. \tag{21}$$

In this case, the leasing cost per linear meter of the deployment site is $c_{le} \approx 11.7$ k€/m and, to obtain the total cost, must be multiplied by the total length of the array (L_{ar}, as shown in Fig. 6). Thus, the LCoE* from Eq. (17) can be now expressed for the specific case as

$$\mathrm{LCoE}^* = \frac{\mathrm{MooEx}^* + L_{ar}c_{le}}{E}, \tag{22}$$

with the absorbed energy E calculated over the 20 years of operational lifespan, as introduced in Section 5.1. The sum of all the considered costs is shown in Fig. 7 for all the array layouts analysed here. Since the layout is symmetric, the costs (and the results in general) can be shown as a function of d_{12} and d_{23}. The jumps in the cost result from changing from one mooring configuration to another one with more sub-components, with the lowest cost at $d_{12} = d_{23} = 2ø$, where the five devices are connected through their KARRATU systems (see Fig. 6.c). Note that the first step in Fig. 7, at 8ø, is due to locating the mooring anchor at 6ø from the device. Thus, 8ø represents the inter-device distance beyond which two (four, due to symmetry) devices are too distant from each other to share a common anchor (as depicted in Fig. 6.b). Furthermore, the highest is in Fig. 7 referring to the scenario where the five devices have independent mooring systems (Fig. 6.a). Finally, the increasing slope of the cost is given by the leasing cost of the site.

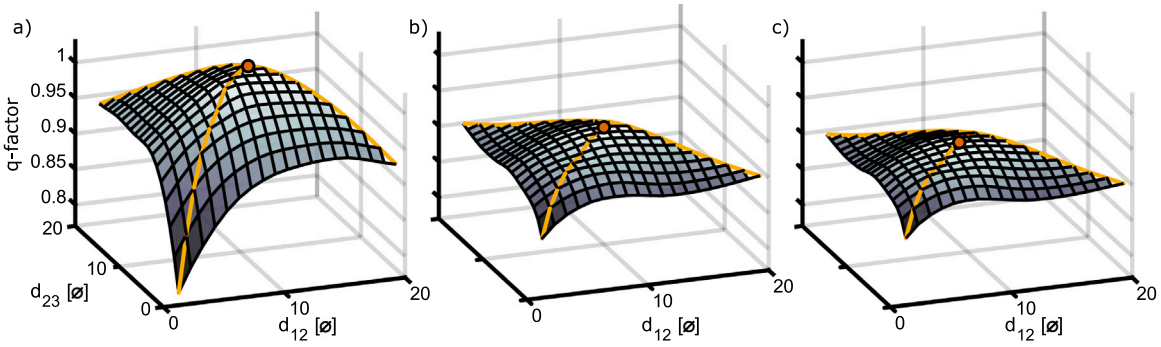

Fig. 8. q-factor obtained from the energy absorbed during the 20 years of lifespan for all the array layouts considered, with different array alignments with respect to the incoming wave: (a) 0°, (b) 45°, and (c) 90°. The orange dot represents the maximum value. The yellow lines in (a), (b), and (c) delineate the cross-sections for the analyses depicted in Fig. 9. Specifically, the equidistant cross-section, where $d_{12} = d_{23}$, is represented by a yellow dashed line, while the maximum distance cross-section, where $d_{12} + d_{23} = 22ø$, is depicted by a solid yellow line.

6. Results & discussion

This section presents and discusses the outcomes derived from the application of the presented CCD methodology for mooring layout design. It is important to note that the results are notably influenced by the costs outlined in the previous section, which may not perfectly align with the actual costs specific to this problem. Consequently, the results presented here should not be interpreted as the definitive optimal array layout for BIMEP, but rather as an illustrative study demonstrating the importance of employing CCD approaches for optimising WEC arrays.

To present the results more clearly, the absorbed energy is expressed by means of the q-factor, as initially introduced in Section 1 (see Eq. (1)). In this light, it should be noted that the energy absorbed by an isolated device during the 20 years of operation is 580 MWh. Thus, Fig. 8 shows the q-factor obtained by the different array layouts and alignments considered. It should be noted that, henceforth, when discussing optimum or maximum energy layouts, the authors are referring to the optimal configuration within the discrete set of considered cases.

One could notice that the highest q-factor is obtained for the array aligned perpendicularly to the wave direction, i.e. the 0° case illustrated Fig. 8.a, for an inter-device distance of $d_{12} = d_{23} = 11ø$ (with a total absorbed power of 2.97 GWh). However, the case shown in Fig. 8.a is also the most varying one among the three, with the minimum absorbed energy at the array configuration with the closest distance, i.e. $d_{12} = d_{23} = 2ø$, due to the destructive interactions. On the contrary, the other two analysed array alignments obtain a less varying but lower energy absorption, with their maximums at 2.71 GWh and 2.70 GWh for Fig. 8.b and .c, respectively. Interestingly, despite the fact that the results are not symmetric, all the maximums happen on an array layout with equidistant inter-device distances.

For further details on the absorbed energy, Fig. 9 shows, all together, the q-factor obtained with the equidistant layouts (Fig. 9.a), i.e. $d_{12} = d_{23}$, and the layouts with the maximum inter-device distance (Fig. 9.b), i.e. the distance from D1 to D5 which, in this case, is 44ø. Note that, for clarity, such two specific cases are also highlighted in Fig. 8.

Fig. 9.a shows that, due to more destructive interactions, the layouts aligned at 0° generate less energy than those aligned at 45° and 90° for inter-device distances of less than (approximately) 4ø, despite being the case obtaining the highest energy absorption (at $d_{12} = d_{23} = 11ø$). One could notice that no strong effect of the interactions can be appreciated on the absorbed energy shown in Fig. 9.a. This is because, depending on the peak period of the sea state, the main interaction effects appear at different inter-device distances and, by considering a large variety of sea-states as in this study, such interaction effects are attenuated. However, it is important to emphasise that, with a sufficiently large inter-device distance, the q-factor shown in Fig. 9.a should converge to 1, representing isolated device cases.

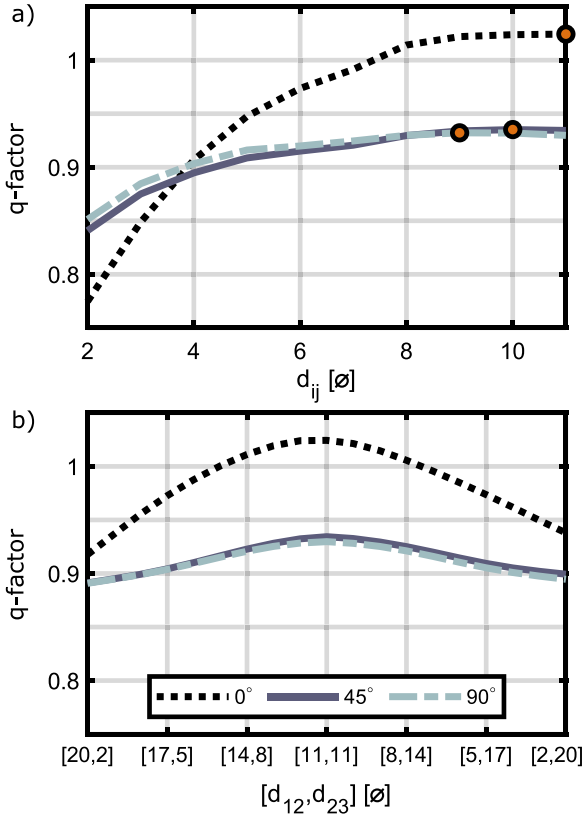

Fig. 9. Cross-section analyses of the absorbed energy. In (a) the equidistant cross-section analysis, represented by a yellow dashed line in Fig. 8, and in (b) the maximum inter-device distance cross-section analysis, depicted with a solid yellow line in Fig. 8.

Furthermore, Fig. 9.b shows that the energy absorbed by the layouts is not symmetric with respect to the equidistant inter-device-distance-axis. In particular, such an asymmetry can be easily appreciated for the 0° layouts, where the cases with larger d_{23} (compared to d_{12}) obtain higher energy absorption (and, hence, q-factor). Thus, the layouts with two pairs of WECs in the corners and the separated device in the middle obtain more energy than the layouts with three devices next to each other in the middle and two separate devices in the corners.

Finally, Fig. 10 shows the LCoE* values (see Eq. (22)) obtained for all the layouts considered. One key aspect to highlight is that the results shown in Fig. 10 closely mirror (inverted, due to the inversion of the z axis) the structure of the costs illustrated in Fig. 7. This is because the absorbed energy does not have much variation (compared to the

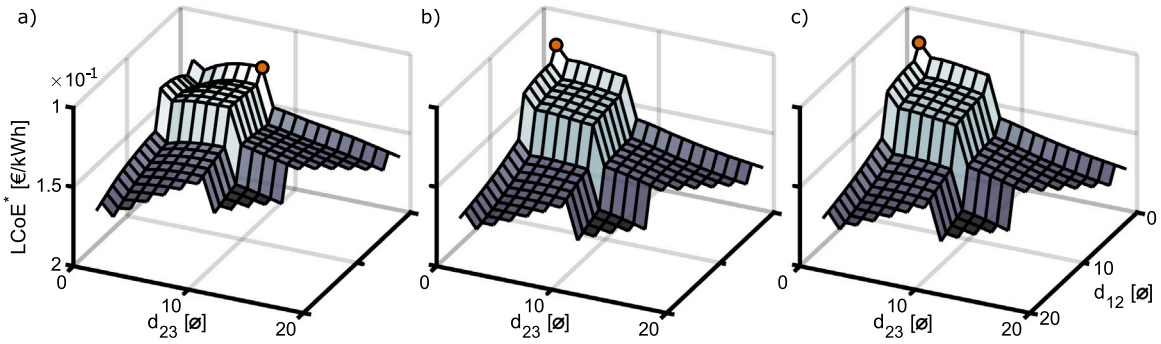

Fig. 10. LCoE* values (obtained as in Eq. (22)) for all the layouts considered, with different alignments between the array and incoming wave: (a) 0°, (b) 45°, and (c) 90°. Note that the z-axis is inverted to improve the visualisation of the results, and the minimum value is highlighted in orange.

cost) and, hence, when dividing the costs by the energy (see Eq. (22)), it retains the shape of the former. Consequently, the optimal case (from an economic perspective) for the arrays aligned at 45° and 90° (Fig. 10.b and .c, respectively) is the case with the lowest costs (despite the fact that is also the case with the lowest energy production), i.e. $d_{12} = d_{23} = 2ø$. Conversely, for the arrays aligned at 0°, the optimal LCoE* is not obtained at the lowest cost case since, as shown in Fig. 8.a, the differences between lowest and highest energy absorption cases in this scenario are larger, counteracting the low cost of the closest inter-device distances. In particular, in Fig. 10.a the optimal case happens at $d_{12} = 2ø$ and $d_{23} = 8ø$ which: (i) on the one hand, is on the limit to not have any device with an independent mooring system which, as explained for Fig. 7, highly increases the cost; and (ii) on the other hand, it represents, from the asymmetric layouts, the distribution with higher energy absorption (two device pairs on the corners and a WEC separated in the middle, i.e. D2 and D3 closer to D1 and D5 than to D3), as explained before for Fig. 9.b.

The optimal LCoE* values in Fig. 10 are 0.119 €/kWh, 0.114 €/kWh, and 0.113 €/kWh for the 0°, 45°, and 90° alignments, respectively. Hence, in the present study, the obtained optimal array for the considered location (BIMEP) should be located in line with respect to the wave direction and with an inter-device distance of $d_{12} = d_{23} = 2ø$. Note that, such an optimal layout (from an economic perspective) corresponds to, as shown in Fig. 9.a, a q-factor of (approximately) 0.85, which means that less energy than five isolated bodies is absorbed.

As mentioned at the beginning of the section, the obtained result does not necessarily mean that such an array is optimal for BIMEP in reality since that is not the aim of the present case study but rather to show how, with the considered CCD approach, it is possible to assess the optimal array layout from an economic perspective, considering the presence of an advanced control strategy. In fact, considering that the obtained LCoE* values only account for the mooring systems (and are already significantly high), it is possible to assume that a different[3] mooring system should probably be considered in this case study, in order to reduce costs, which would change the obtained results.

Finally, to illustrate the constraint handling mechanism, Fig. 11 shows the position and velocity for three of the five devices for the economically optimal layout (i.e. $d_{12} = d_{23} = 2ø$ and in-line with the wave direction) for the sea state with highest significant wave height ($H_s = 3.5$ m and $T_p = 13.5$ s). One could notice that the position of all the devices is within the constraints imposed by the control strategy.

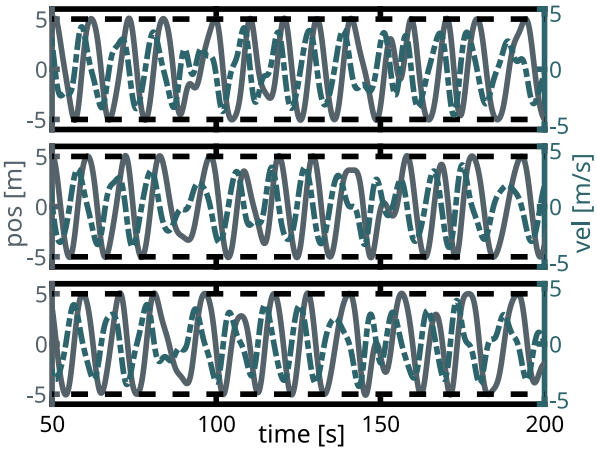

Fig. 11. Position (solid grey line) and velocity (dashed blue line) of D1, D3, and D5 for the highest SS and the economically optimal layout.

7. Conclusion

The current study proposes a CCD methodology for array layout design from an economic perspective, with an application case aimed at demonstrating the effectiveness of such CCD algorithm in a realistic context. To this end, the current study considers (i) 20 years of actual sea states (and their historical probabilities) at the BIMEP test site to compute the WEC array energy production, (ii) a realistic WEC (MARMOK-A-5-like device) that was deployed at such test site for two years, and (iii) a mooring configuration (termed KARRATU) that was developed for such device. Additionally, the study meticulously includes the mooring costs by separately analysing all the components of the KARRATU system, deriving the costs using insights from offshore floating wind literature.

The results provide clear insights into the energy absorption by the different array layouts considered (changing the inter-device distances and alignments with respect to the incoming waves). The highest energy absorption is observed when the array is aligned perpendicularly to the wave direction, with an equidistant inter-device distance of $d_{12} = d_{23} = 11ø$. However, the study suggests that the optimal array layout, from an economic perspective, should align with the wave direction and maintain an inter-device distance of $d_{12} = d_{23} = 2ø$, Note that such results coincide with those obtained in similar studies in the literature, such as [33] where some of the results from the Pareto front indicate that the bodies should be in line with the wave direction or that the WECs should be as close to each other as possible to reduce costs.

This study underscores the critical importance of adopting a CCD approach to assess optimal array layouts from an economic perspective while integrating advanced control strategies. It highlights a significant observation — the optimal layout for economic factors might not align with the optimal choice based solely on technical factors, such as energy absorption, as demonstrated in the presented case study. In fact, for the study at hand, it was counterintuitive that one of the most

[3] Note that, as introduced in Section 5.3, the costs of the considered mooring systems come from an offshore floating wind study, due to the lack of information on this matter for WECs.

economically favourable layouts was among the least energy-efficient. While these specific findings may not prescribe the ideal BIMEP array layout in practice, they strongly underscore the necessity of employing a CCD approach, as presented in this study, when designing wave energy converter arrays. This approach ensures that array designs consider not only energy absorption but also economic considerations, contributing to a more comprehensive and balanced decision-making process.

It should be noted that the results obtained in the current study are not necessarily transferable to other types of WECs since they highly depend on the considered costs, location, etc. However, the proposed CCD approach can be applied to any type of WEC, by properly defining its dynamics, costs, and mooring configuration.

Finally, it is essential to reiterate that these findings are not necessarily indicative of the actual optimal array for BIMEP in practice, as this was not the primary aim of the case study. In fact, in order to correctly address the problem of optimising an array for a given location, several aspects should be improved in the proposed study. Such limitations include, among others, a linear representation of the WEC dynamics, a simple (and not necessarily realistic) representation of the WEC costs, and a limited possibility of array layouts (since a single layout with five devices in line is considered). Future work includes addressing the aforementioned limitations of the study in order to improve the usefulness of the CCD tool.

CRediT authorship contribution statement

Yerai Peña-Sanchez: Conceptualization, Data curation, Formal analysis, Funding acquisition, Investigation, Methodology, Software, Validation, Writing – original draft, Writing – review & editing. **Demián García-Violini:** Conceptualization, Investigation, Methodology, Validation, Writing – original draft, Writing – review & editing. **Markel Penalba:** Conceptualization, Funding acquisition, Project administration, Supervision, Writing – original draft, Writing – review & editing. **Ander Zarketa-Astigarraga:** Methodology, Supervision, Validation, Writing – review & editing. **Francesco Ferri:** Methodology, Resources, Software, Writing – review & editing. **Vincenzo Nava:** Funding acquisition, Methodology, Supervision, Writing – review & editing. **John V. Ringwood:** Methodology, Supervision, Validation, Writing – review & editing.

Declaration of competing interest

The authors declare the following financial interests/personal relationships which may be considered as potential competing interests: Yerai Pena-Sanchez reports financial support was provided by European Union's Horizon 2020 research and innovation programme. If there are other authors, they declare that they have no known competing financial interests or personal relationships that could have appeared to influence the work reported in this paper.

Acknowledgements

The authors at Mondragon University are funded by the research project PID2021-124245OA-I00 funded by MCIN/AEI/10.13039/501100011033 and by ERDF A way of making Europe, and the research project funded by the Basque Government's ELKARTEK 2022 program under the grant No. KK-2022/00090. In addition, Yerai Peña-Sanchez is funded by the European Union's Horizon 2020 research and innovation programme under the Marie Sklodowska-Curie grant agreement N°10103429, Demián García-Violini is supported by the Agencia I+D+i from the Government of Argentina under grant PICT-2021-I-INVI-00190, and John Ringwood is supported by Science Foundation Ireland (SFI) through the MaREI Centre for Energy, Climate and Marine under Grant No. 12/RC/2302_P2. Vincenzo Nava's work is funded by the Spanish Ministry of Science and Innovation projects with references TED2021-132783B-I00, PID2019-108111RB-I00 (FEDER/AEI); the Spanish Ministry of Economic Affairs and Digital Transformation project with reference MIA.2021.M04.0008; the "BCAM Severo Ochoa" accreditation of excellence CEX2021-001142-S/MICIN/AEI/10.13039/501100011033; and the Basque Government, Spain through the BERC 2022–2025 program.

References

[1] UN, Adoption of the paris agreement, 2015, URL https://www.iea.org/publications/freepublications/publication/ElectricityInformation2017Overview.pdf.
[2] IPCC, Synthesis Report of the IPCC Sixth Assessment Report (AR6), Tech. Rep., Intergovernmental Panel on Climate Change (IPCC), ISBN: 978-92-9169-151-7, 2023, URL https://report.ipcc.ch/ar6syr/pdf/IPCC_AR6_SYR_SPM.pdf.
[3] IPCC, Global Warming of 1.5∘C, Tech. Rep., Intergovernmental Panel on Climate Change (IPCC), ISBN: 978-92-9169-151-7, 2018.
[4] IRENA, Future of Wind: Deployment, Investment, Grid Integration and Socio-Economic Aspects (A Global Energy Transformation Paper), Tech. Rep., International Renewable Energy Agency, Abu Dhabi, ISBN: 978-92-9260-121-8, 2019, Available in https://www.irena.org/publications/2019/Apr/Global-energy-transformation-A-roadmap-to-2050-2019Edition.
[5] S. Bouckaert, A.F. Pales, C. McGlade, U. Remme, B. Wanner, Net Zero by 2050: A Roadmap for the Global Energy Sector, Tech. rep., International Energy Agency, Paris, 2021, p. 224, URL https://www.iea.org/reports/net-zero-by-2050.
[6] Ocean Energy Europe, 2030 Ocean Energy Vision, Tech. rep., 2020, URL https://www.oceanenergy-europe.eu/wp-content/uploads/2020/10/OEE_2030_Ocean_Energy_Vision.pdf.
[7] NREL, Marine Energy in the United States : An Overview of Opportunities, Tech. Rep. February, 2021, URL https://www.nrel.gov/docs/fy21osti/78773.pdf.
[8] B. Guo, J.V. Ringwood, A review of wave energy technology from a research and commercial perspective, IET Renew. Power Gener. 15 (14) (2021) 3065–3090, http://dx.doi.org/10.1049/rpg2.12302.
[9] K. Wang, Z. Wang, S. Sheng, Y. Zhang, Z. Wang, Y. Ye, W. Wang, H. Lin, Z. Huang, A method for large-scale WEC connecting to island isolated microgrid based on multiple small power HPGSs, Renew. Energy (2023) 119330.
[10] F. Fusco, G. Nolan, J.V. Ringwood, Variability reduction through optimal combination of wind/wave resources–An Irish case study, Energy 35 (1) (2010) 314–325.
[11] S. Astariz, G. Iglesias, Output power smoothing and reduced downtime period by combined wind and wave energy farms, Energy 97 (2016) 69–81.
[12] W. Sasaki, Predictability of global offshore wind and wave power, Int. J. Mar. Energy 17 (2017) 98–109.
[13] A. Pecher, J.P. Kofoed, Handbook of Ocean Wave Energy, Springer Nature, 2017.
[14] IRENA, OEE, Scaling Up Investments in Ocean Energy Technologies, Tech. rep., International Renewable Energy Agency, Abu Dhabi, 2023.
[15] F. Teixeira-duarte, D. Clemente, G. Giannini, P. Rosa-santos, F. Taveira-pinto, Review on layout optimization strategies of offshore parks for wave energy converters, Renew. Sustain. Energy Rev. 163 (May) (2022) 112513, http://dx.doi.org/10.1016/j.rser.2022.112513.
[16] P.B. Garcia-Rosa, G. Bacelli, J.V. Ringwood, Control-informed optimal array layout for wave farms, IEEE Trans. Sustain. Energy 6 (2) (2015) 575–582, http://dx.doi.org/10.1109/TSTE.2015.2394750.
[17] M. Penalba, T. Kelly, J. Ringwood, Using NEMOH for modelling wave energy converters: A comparative study with WAMIT, in: 12th European Wave and Tidal Energy Conference, EWTEC, 2017.
[18] WAMIT, WAMIT, 2023, https://www.wamit.com, Online accessed 1-Jun-2023.
[19] A. Babarit, Impact of long separating distances on the energy production of two interacting wave energy converters, Ocean Eng. 37 (8–9) (2010) 718–729.
[20] A. De Andrés, R. Guanche, L. Meneses, C. Vidal, I. Losada, Factors that influence array layout on wave energy farms, Ocean Eng. 82 (2014) 32–41.
[21] S. Bozzi, M. Giassi, A.M. Miquel, A. Antonini, F. Bizzozero, G. Gruosso, R. Archetti, G. Passoni, Wave energy farm design in real wave climates: the Italian offshore, Energy 122 (2017) 378–389.
[22] A numerical study on the hydrodynamic impact of device slenderness and array size in wave energy farms in realistic wave climates, Ocean Eng. 142 (2017) http://dx.doi.org/10.1016/j.oceaneng.2017.06.047.
[23] A. Mérigaud, J.V. Ringwood, Improving the computational performance of nonlinear pseudospectral control of wave energy converters, IEEE Trans. Sustain. Energy 9 (3) (2018) 1419–1426, http://dx.doi.org/10.1109/TSTE.2017.2786045.
[24] M. Garcia-Sanz, Control co-design: An engineering game changer, Adv. Control Appl.: Eng. Ind. Syst. 1 (1) (2019) e18.
[25] R.G. Coe, G. Bacelli, S. Olson, V.S. Neary, M.B.R. Topper, Initial conceptual demonstration of control co-design for WEC optimization, J. Ocean Eng. Mar. Energy 6 (4) (2020) 441–449, http://dx.doi.org/10.1007/s40722-020-00181-9.
[26] Y. Peña-Sanchez, D. García-Violini, J.V. Ringwood, Control co-design of power take-off parameters for wave energy systems, IFAC-PapersOnLine 55 (27) (2022) 311–316, http://dx.doi.org/10.1016/j.ifacol.2022.10.531.

[27] K. Budal, Theory for absorption of wave power by a system of interacting bodies, J. Ship Res. 21 (04) (1977) 248–254.
[28] P. Ricci, A. Rico, F. Boscolo, J.L. Villate, Design , modelling and analysis of an integrated mooring system for wave energy arrays, in: 4th International Conference on Ocean Energy, Dublin, Ireland, 2012.
[29] B. Howey, K.M. Collins, M. Hann, G. Iglesias, R.P. Gomes, J.C. Henriques, L.M. Gato, D. Greaves, Compact floating wave energy converter arrays: Inter-device mooring connectivity and performance, Appl. Ocean Res. 115 (2021) 102820.
[30] X. Shao, J.W. Ringsberg, H.-D. Yao, Z. Li, E. Johnson, G. Fredriksson, A comparison of two wave energy converters' power performance and mooring fatigue characteristics–One WEC vs many WECs in a wave park with interaction effects, J. Ocean Eng. Sci. (2023).
[31] J.B. Thomsen, F. Ferri, J.P. Kofoed, K. Black, Cost optimization of mooring solutions for large floating wave energy converters, Energies 11 (1) (2018) 159.
[32] Y. Peña-Sanchez, D. García-Violini, A. Zarketa, M. Penalba, V. Nava, J.V. Ringwood, Wave energy converter array layout control co-design for different mooring configurations, in: 15th European Wave and Tidal Energy Conference, Bilbao, Spain, 2023, p. 531, http://dx.doi.org/10.36688/ewtec-2023-531, no. September.
[33] D.R. David, A. Kurniawan, H. Wolgamot, J.E. Hansen, D. Rijnsdorp, R. Lowe, Nearshore submerged wave farm optimisation: A multi-objective approach, Appl. Ocean Res. 124 (2022) 103225.
[34] M. Giassi, V. Castellucci, M. Göteman, Economical layout optimization of wave energy parks clustered in electrical subsystems, Appl. Ocean Res. 101 (2020) 102274.
[35] M. Neshat, B. Alexander, M. Wagner, A hybrid cooperative co-evolution algorithm framework for optimising power take off and placements of wave energy converters, Inform. Sci. 534 (2020) 218–244.
[36] T.F. Ogilvie, Recent progress toward the understanding and prediction of ship motions, in: 5th Symposium on Naval Hydrodynamics, Vol. 1, Bergen, Norway, 1964, pp. 2–5.
[37] J. Falnes, Ocean Waves and Oscillating Systems: Linear Interactions Including Wave-Energy Extraction, Cambridge Univ. Press, ISBN: 9780511754630, 2002.
[38] D. García-Violini, Y. Peña-Sanchez, N. Faedo, J.V. Ringwood, An energy-maximising linear time invariant controller (LiTe-Con) for wave energy devices, IEEE Trans. Sustain. Energy 11 (4) (2020) 2713–2721.
[39] H. Kagemoto, D.K. Yue, Interactions among multiple three-dimensional bodies in water waves: an exact algebraic method, J. Fluid Mech. 166 (1986) 189–209.
[40] J.C. McNatt, V. Venugopal, D. Forehand, A novel method for deriving the diffraction transfer matrix and its application to multi-body interactions in water waves, Ocean Eng. 94 (2015) 173–185.
[41] N. Faedo, S. Olaya, J.V. Ringwood, Optimal control, MPC and MPC-like algorithms for wave energy systems: An overview, IFAC J. Syst. Control 1 (2017) 37–56.
[42] R. Genest, J.V. Ringwood, A critical comparison of model-predictive and pseudospectral control for wave energy devices, J. Ocean Eng. Mar. Energy 2 (2016) 485–499.
[43] D. Garcia-Violini, J.V. Ringwood, Energy maximising robust control for spectral and pseudospectral methods with application to wave energy systems, Internat. J. Control 94 (4) (2021) 1102–1113.
[44] D. García-Violini, M. Farajvand, C. Windt, V. Grazioso, J.V. Ringwood, Passivity considerations in robust spectral-based controllers for wave energy converters, in: 2021 XIX Workshop on Information Processing and Control, RPIC, IEEE, 2021, pp. 1–6.
[45] G. Bacelli, J.V. Ringwood, Numerical optimal control of wave energy converters, IEEE Trans. Sustain. Energy 6 (2) (2015) 294–302.
[46] S. Barstow, G. Mørk, D. Mollison, J. Cruz, The wave energy resource, in: Ocean Wave Energy, Springer, 2008, pp. 93–132.
[47] A. Ulazia, M. Penalba, G. Ibarra-Berastegui, J. Ringwood, J. Saénz, Wave energy trends over the Bay of Biscay and the consequences for wave energy converters, Energy 141 (2017) 624–634.
[48] A. Zarketa-astigarraga, M. Agirre-aspiazu, A. Martin-mayor, K. Castro, M. Martinez-agirre, B. De Miguel, M. Penalba, Air turbine optimisation for OWC wave energy converters : Sensitivity of realistic wave climates, in: 15th European Wave and Tidal Energy Conference, Bilbao, Spain, 2023, p. 493, http://dx.doi.org/10.36688/ewtec-2023-493, no. September.
[49] S. Weller, D.N. Parish, D. Trnroos, L. Johanning, Open sea OWC motions and mooring loads monitoring at BiMEP, in: Proceedings of the 12th European Wave and Tidal Energy Conference, Cork, Ireland, 2017, pp. 1–10, no. August.
[50] A.A. Carrelhas, L.M. Gato, J.C. Henriques, A.F. Falcão, J. Varandas, Test results of a 30 kW self-rectifying biradial air turbine-generator prototype, Renew. Sustain. Energy Rev. 109 (2019) 187–198.
[51] P. Thies, L. Johanning, P. Mcevoy, A novel mooring tether for peak load mitigation: Initial performance and service simulation testing, Int. J. Mar. Energy 7 (2014) http://dx.doi.org/10.1016/j.ijome.2014.06.001.
[52] F. Khalid, A. Rhahida, L. Johanning, B. de Miguel, D. Tornroos, P. Goodwin, Mooring Open-Sea Operating Data Analysis, Tech. Rep. OPERA project D2.2, University of Exeter, 2019, pp. 1–64, URL http://opera-h2020.eu/wp-content/uploads/2019/09/OPERA_D2.2_Mooring-open-sea-data-analysis_UNEXE_20190621_v1.2.pdf.
[53] T. Bloise Thomaz, D. Crooks, E. Medina-Lopez, L. van Velzen, H. Jeffrey, J. Lopez Mendia, R. Rodriguez Arias, P. Ruiz Minguela, O&M models for ocean energy converters: Calibrating through real sea data, Energies 12 (13) (2019) http://dx.doi.org/10.3390/en12132475, URL https://www.mdpi.com/1996-1073/12/13/2475.
[54] K. Xu, K. Larsen, Y. Shao, M. Zhang, Z. Gao, T. Moan, Design and comparative analysis of alternative mooring systems for floating wind turbines in shallow water with emphasis on ultimate limit state design, Ocean Eng. 219 (2021) 108377.
[55] A. Pillai, T. Gordelier, P. Thies, C. Dormenval, B. Wray, R. Parkinson, L. Johanning, Anchor loads for shallow water mooring of a 15 MW floating wind turbine—Part I: Chain catenary moorings for single and shared anchor scenarios, Ocean Eng. 266 (2022) 111816.
[56] I. Touzon, V. Nava, B. de Miguel, V. Petuya, A comparison of numerical approaches for the design of mooring systems for wave energy converters, J. Mar. Sci. Eng. 8 (7) (2020) 523.